Rapid and controllable design of robust superwettable microchips by a click reaction for efficient o-phthalaldehyde and glucose detection

Huang, Jianying; Yang, Hui; Mao, Jiajun; Guo, Fang; Cheng, Yan; Chen, Zhong; Wang, Xiaoqin; Li, Xiao; Lai, Yuekun

2019

Huang, J., Yang, H., Mao, J., Guo, F., Cheng, Y., Chen, Z., Wang, X., Li, X. & Lai, Y. (2019). Rapid and controllable design of robust superwettable microchips by a click reaction for efficient o-phthalaldehyde and glucose detection. ACS Biomaterials Science & Engineering, 5(11), 6186-6195. https://dx.doi.org/10.1021/acsbiomaterials.9b00821

https://hdl.handle.net/10356/150778

https://doi.org/10.1021/acsbiomaterials.9b00821

Rapid and controllable design of robust superwettable microchips by click reaction for efficient o-phthalaldehydes and glucose detection

Jianying Huang[a], Hui Yang[a,b], Jiajun Mao[a], Fang Guo[b], Yan Cheng[b], Zhong Chen[c], Xiaoqin Wang[b], Xiao Li[a], Yuekun Lai[a,b]*

[a] College of Chemical Engineering, Fuzhou University, Fuzhou 350116, P. R. China.

[b] National Engineering Laboratory for Modern Silk, College of Textile and Clothing Engineering, Soochow University, Suzhou 215123, P. R. China.

[c] School of Materials Science and Engineering, Nanyang Technological University, 50 Nanyang Avenue, Singapore.

Corresponding Authors E-mail: yklai@fzu.edu.cn

Abstract

Superwettable patterns with superhydrophobic and superhydrophilic units have the capacity of enriching and absorbing microdroplet for multi-functional biosensing. Combining the advantages of superwettable micropatterns and rapid click reaction, we first prepared a film using propargyl methacrylate-ethylene dimethacrylate (PM-EDMA), then created superhydrophobic-superhydrophilic micropattern by a rapid thiol-yne click reaction. Due to the high wettability contrast, water droplets tend to be anchored in the superhydrophilic region. Molecules dissolved in a water droplet are therefore uniformly enriched in the superhydrophilic region after evaporation because of the Malangoni effect. This provides a rational strategy to develop novel patterned microchips for sensing applications. Combining with fluorescence imaging technology, the Ti superwettable microchip can be used to detect o-phthalaldehyde (OPA) in water, with a detection limit as low as 10^{-7} mol L^{-1}. In addition, taking advantage of the oxidative color rendering ability of glucose, the microchip, when fabricated on glass substrate, can realize reuseable glucose detection with a detection limit of 2 mM within 15 min.

Keywords: Superhydrophobic-superhydrophilic; Microchips; Click reaction; Fluorescence detection; Glucose detection

Introduction

Namib Desert beetle's hydrophilic texture on their wings and superhydrophobic groove on their back work together to draw steam from the the ambience. As the water droplets accumulate in the hydrophilic zone, they roll down the arched back and go into the desert beetle's mouth.[1] Besides Namib Desert beetle, there are many other creatures in nature with superhydrophobic-superhydrophilic surface, such as conical spine of cactus, the peristome surface of Nepenthes alata

and the surface of spider silk, which enable efficient water collection from air.[2-5] Inspired by nature, many materials with extreme superwettability patterns have been developed for various applications,[6-9] including fog collection,[10-12] selective cell adhesion,[13-15] microfluidics[16, 17] and microarray for cell.[18, 19]

A series of approaches to prepare superhydrophobic-superhydrophilic micropatterns have been reported over the last decades. The micropatterns can be obtained by UV decomposition method,[13, 20, 21] as demonstrated by Ishizaki et al. They prepared superhydrophobic films using chemical vapor deposition method, then irradiated ultraviolet light on the film through a photomask to fabricate superhydrophobic-superhydrophilic patterns.[8] Laser machining can also be uesd to prepare micropatterns, as shown by Kostal et al., who deposited a Teflon-like polymer on the superhydrophilic surface by a plasma process. Then the Teflon-like superhydrophobic coating was selectively removed by femtosecond laser ablation to generate the micropattern.[22] Another way to generate superwettable micropattern is inkjet printing.[23, 24] Recent effort in this area has been shifted to more flexible and powerful functionalities and possibilities including high-throughput cell patterns,[25-27] biomedical screening,[28-30] and biological assay et al.[31-33]

Due to the surface energy difference between superhydrophobic region and superhydrophilic region, micropatterns show excellent ability in controlling water droplets.[34-36] It is easy to imagine that water solution droplets tend go from the superhydrophobic region to superhydrophilic region, and stay there stably. The anchored droplets can be exploited for a series of advantages such as simplifying reaction procedure, accelerating homogeneous mixing rate, generating uniform deposition and improving detection sensitivity. The droplet-based micropatterns is a miniaturized laboratory, which can perform both bio-chemical reactions and biological analysis.[37-40] A number

of superwettable microchips have been developed and applied in different detections, including surface-enhanced Raman scattering,[41, 42] colorimetric,[23] and fluorescence enhancement effect.[43-45]

However, the conventional method to prepare micropattern requires complicated preparation process, long cycle and chemical consumption. In the curent work, due to UV-induced thiol-yne click reaction can realize regional surface modificationw, we propose the use thiol-yne click reaction towards the creation of the superhydrophobic-superhydrophilic micropatterns. This approach combines the typical characteristics of the click reaction with the advantages of photoinitiation. It has the advantages of rapid reaction, mild conditions required, and is therefore suitable for a variety of functional groups. More importantly, we are going to demonstate microchips containing such highly contrasted wettability patterns toward the detection of OPA and glucose. The generated superwettable microchips have excellent mechanical durability and acid-base resistance properties.

Materials and Method

Materials and Reagents. Propargyl methacrylate (PM, 98%) was purchased from Alfa, ethylene dimethacrylate (EDMA, 98%), potassium iodide (KI) and 2,2-Dimethoxy-2-phenylacetophenone (DMPAP, ≥99%) were purchased from Aladdin, ammonium fluoride (NH_4F, AR), 3-mercaptopropionic acid (≥98%) and OPA (99%) were purchased from Macklin, 1-decanol (98%) was purchased from Yonghua chemical technology Co. Ltd., 1H,1H,2H,2H-perfluorodecanethiol (97%) and 1-dodecanethiol were purchased from Sigma-Aldrich, 2-mercaptoethanol (≥98%) was purchased from Tci, 2-Aminoethanethiol Hydrochloride (≥98%) was purchased from Adamas, glucose (AR) and cyclohexanol (97%) were purchased from Sinopharm chemical reagent Co. Ltd.,

glucose oxidase (GO_x, 100 U mg^{-1}) was purchased from BBI. All chemicals were used as received without further purification.

Polymerization mixtures: Smooth PM-EDMA film (sample 1): 60 wt.% PM, 40 wt.% DMA and DMPAP (1 wt.% with respect to monomers). Rough PM-EDMA film (sample 2-6): 24 wt.% PM, 16 wt.% EDMA, DMPAP (1 wt.% with respect to monomers) and different concentrations of 1-decanol and cyclohexanol: sample 2: 1-decanol (60 wt.%); sample 3: 1-decanol (50 wt.%) and cyclohexanol (10 wt.%); sample 4: 1-decanol (40 wt.%) and cyclohexanol (20 wt.%); sample 5: 1-decanol (20 wt.%) and cyclohexanol (40 wt.%); sample 6: cyclohexanol (60 wt.%).

Surface modification of titanium sheets and glass plates. The glass plates (2.5 cm × 2.5 cm) and titanium sheets (2.5 cm × 2.5 cm) were sequentially washed with acetone, ethanol and deionized water with ultrasonication. The titanium sheets were anodized in NH_4F electrolyte at 50 V for 1 h using Pt as the counter electrode.

Preparation of PM-EDMA film. A PM-EDMA film with terminal alkyne group was prepared by UV curing method. 30 μL PM-EDMA mixture was dropped-cast onto the titanium substrte, the substrate was then cover with a clean glass. Four 12.5 μm thick Teflon strips were placed between the titanium substrate and the glass cover. The whole setup was exposed to 260 nm UV light (12 mW cm^{-2}) for 15 min to obtain PM-EDMA polymer film. Once the process of UV polymerization curing was completed, the cover was opened, and the cured film was immersed in methanol for 30 min to clean the unreacted agents.

Fabrication of superwettable micropattern via thiol-yne reaction. Superhydrophobic-superhydrophilic micropatterns were constructed by UV irradiation via thiol-yne click reaction. The PM-EDMA film was firstly wetted with a solution containing 15 vol.% 2-mercaptoethanol of ethanol, and covered with a photomask, before it was exposed to 260 nm UV light (12 mW cm^{-2})

for 5 min at room temperature. The exposed region completed the grafting reaction and turned to superhydrophilicity while the non-exposed region remain unchanged. The selectively grafted film was washed with acetone to remove unreacted solvent. Then the film was wetted with a solution containing 5 vol.% 1H, 1H, 2H, 2H-Perfluorodecanethiol of acetone, covered with quartz glass and exposed to UV light for another 5 min. So the non-reaction region (non-exposed region) tranformed to superhydrophobicity, then it was washed with acetone to remove unreacted solvent.

Characterization. The morphology of samples was viewed by a field emission scanning electron microscope (FESEM, HitachiS-4800) at 3.0 kV. Fourier transform infrared (FTIR) spectrophotometer at a range of 4000-400 cm^{-1} were detected on a Varian Scimitar 1000 spectrophotometer. Elemental analysis was carried out by an energy dispersive X-ray spectrometer (EDS) fitted to the SEM. The chemical components were detected by a Kratos Axis-Ultra HSA X-ray photoelectron spectrometer (XPS) with a 100 W $Al_{K\alpha}$ X-ray source and a base pressure of ~4×10^{-9} mbar. A Raman spectrometer (HORIBA JOBIN YVON, HR800) was used to analyse the Raman spectrum. A contact angle meter system (Krüss DSA100, Germany) was applied to examine the wetting properties of water droplets. The volume of droplets applied for the static water contact angle (WCA) measurement was 6 μL. ^1H NMR spectra were observed on a Varian spectrometer (Unity INOVA 400NB) at room temperature with a DMSO as the solvent. Fluorescent images were recorded with inverted fluorescence microscopy (FV1000).

Fluorescence detection of o-phthalaldehydes (OPA). Droplets in the size of 2 μL with different concentration of OPA were added onto microdots of different diameters (1000, 500 and 400 μm). Fluorescence images were acquired from a inverted fluorescence microscopy (FV1000) after evaporation for several hours in dark.

Colorimetric detection of glucose. Hydrogen peroxide (H_2O_2) is produced by glucose oxidase （GO_x） oxidation of glucose, the final coloration by H_2O_2 oxidation of KI is increasing as the increase of glucose concentration. 2 μL GO_x (15 Um L^{-1}) and 2 μL KI (0.6 M) were dropped to the microchips, then 1 μL glucose droplet with various concentrations of 0, 2, 4, 8, 10, 25 and 50 mM was dropped onto the microdots. Finally, the pictures were recorded after 15 min reaction and the image J analysis was applied to assist the analysis of the results.

Results and Discussion

WCA and morphology of PM-EDMA film. As described earlier, smooth and rough PM-EDMA films on the titanium dioxide substrate were prepared. **Figure S1** shows that the smooth sample 1 had a WCA of 77.1 ± 2.9°, which indicating a slightly hydrophilicity. Samples 2-6 were rough PM-EDMA films, they showed WCA of 142.5 ± 5.6°, 134.2 ± 6°, 118.4 ± 3.5°, 108.4 ± 5.1°, 100 ± 3.6°, respectively. Therefore, when only PM and EDMA are in the PM-EDMA film, the film showed weak hydrophilicity. When 1-decanol and cyclohexanol were added into mixtures with different proportions, the resulting PM-EDMA films exhibited hydrophobicity, and the WCA gradually decreased with the increase of cyclohexanol and decrease of 1-decanol.

Figure S2A-F shows the surface morphology of different PM-EDMA films. Sample 1 is smooth, and samples 2-5 show interconnected spherical structure while there is no obvious bulges or spherical particles on sample 6. With the increase of cyclohexanol and decrease of 1-decanol in samples 2-5, the diameter of globular particles gradually decreased, and this was accompanied with the decrease of WCA. The presence of 1-decanol and cyclohexanol in the polymerizd mixture could induce phase separation when the cross-linked polymer chains aggregate to a critical size, further forming interconnected globules.[46, 47] However, sample 4 that contains 24 wt.% PM, 16 wt.

% EDMA, 20 wt.% cyclohexanol and 40 wt.% 1-decanol has the most stable WCA and the most uniform spherical particle distribution. Therefore this sample was selected for the subsequent experiments. **Figure S3** shows the cross-section SEM image of PM-EDMA films, the Ti surface was coverd with a loose and uniform layer.

Wettability transition. The resultant PM-EDMA film can realize the surface wettability transition by being further modified with different thiol solution. **Figure 1** illustrates the schematic diagram of turning the PM-EDMA film into superhydrophilic or superhydrophobic state via UV-induced thiol-yne click reaction chemistry. The PM-EDMA film contains a lot of C≡C, which provides the reaction groups for thiol-yne reaction. More details will be shown in later disscussion. As **Figure 2**A shows, the surface with the reactive groups (R groups) was obtained by the click reaction between C≡C triple bond of PM-EDMA film and the sulfydryl group of thiol solution. **Figure 2**B shows the change of WCA of surface after PM-EDMA film reacting with different thiol solutions with different R groups. After 300 s UV inradition, reaction between PM-EDMA film and 1-dodecanethiol (red)/1H, 1H, 2H, 2H-perfluorodecanethiol (black) completed, and the resulting WCA approaches 162.5 ± 2.5° and 168.2 ± 2.8°, respectively. On the other hand, the superhydrophilicity of the surface is endowed by the modification of the PM-EDMA film with 3-mercaptopropionic acid (blue)/cysteamine (purple)/2-mercaptoethanol (green). The WCA reaches as low as 5.1 ± 3.5°, 4.9 ± 2.9° or 3.6 ± 2.4°, respectively. Therefore, when the R is -COOH, -OH and -NH_2 groups, the surface shows superhydrophilicity, while when the R group is alkyl and perfluoro groups, the surface shows superhydrophobicity. In order to obtaine the best superhydrophobicity and superhydrophilicity, 1H, 1H, 2H, 2H-perfluorodecanethiol and 2-mercaptoethanol were chose to perform subsequent investigation.

The SEM images and WCA of samples after each step are exhibited in Figure 2C. The surface of titanium dioxide with a uniformly distributed nodule structure displays a WCA of 9.7 ± 2.3°. There was no obvious morphology change after reacting with 1-dodecanethiol, 1H, 1H, 2H, 2H-perfluorodecanethiol, 3-mercaptopropionic acid, 2-mercaptoethanol, cysteamine.

In addition, we investigated the effect of UV light irradiation time and photoinitiator during thiol-yne click reaction. As shown in **Figure S4**A, it took 300 s UV irradiation to transform PM-EDMA film into a superhydrophilic (3.6 ± 2.5°, blue) surface. The red curve suggests that thiol-yne recation also occurred without DMPAP, but the black curve indicates that there was no reaction happening without UV irradiation. Besides, as shown in Figure S4B, the thiol-yne reaction can work in various kinds of solvents. Meanwhile, the same PM-EDMA film, 125 μm in thickness, was also applied in the glass substrate. As displayed in **Figure S5**, the WCA of PM-EDMA film on the glass subtrate is 125.3 ± 2.8°, while the superhydrophobic and superhydrophilic samples showed WCA of close to 0° and 165.6 ± 3.1°, respectively.

Surface chemical composition analysis. We have investigated the relationship between surface roughness and wettability. As shown in **Figure 3A**, the 3D AFM image of PM-EDMA film whose RMA value is about 350 nm shows an uneven distribution of granular morphology. The 3D AFM images of superhydrophobic and superhydrophilic samples are displayed in Figure 3B and C, the roughness of superhydrophobic sample was measured to be 380 nm whereas the RMS value of superhydrophilic sample was around 367 nm. There was little change in the surface morphologies before and after the click reaction.

In order to illustrate the effect of surface chemistry on wetting behavior, elemental composition and distribution was investigated by EDS. As shown in Figure 3D, the atomic percentage of C, O and Ti elements on the surface of PM-EDMA film was 35.59%, 36.96% and

27.45 at%. Figure 3E and F show the EDS result of the superhydrophobic and superhydrophilic samples. Both samples contained C, O and Ti elements. The appearance of the S peak in the two samples demonstrates successful grafting of the two thiols on the PM-EDMA film. The atomic percentage of F at the superhydrophobic sample was 19.09% at which belongs to 1H, 1H, 2H, 2H-perfluorodecanethiol.

We also used XPS to analyze the chemical bonding information in the whole synthesis process. As shown in **Figure 4**A, the wide XPS spectra of the PM-EDMA film (black) suggest that the film was mainly composed of C and O elements. The C 1s high resolution spectrum in Figure 4B shows peaks at 284.7 eV, 286.1 eV and 288.6 eV, which are overlapped signals of C-C, C-O and C=O bonds, respectively. Besides, the sharp peak belonging to the C≡C bands (2135 cm^{-1}) can be observed on the PM-EDMA film from the FT-IR image in **Figure S6**. This confirms that the film contains C≡C groups that are reactive for thiol-yne click reaction.

After the two-step thiol-yne click chemical reactions, the chemical composition of the surface superhydrophobic and superhydrophilic samples showed difference from each other. As shown in Figure 4A, new signal belong to S was observed in both superhydrophilic (blue) and superhydrophobic (red) samples. While the F peak only appeared in the superhydrophobic sample, which indicates the successful grafting of 1H, 1H, 2H, 2H-perfluorodecanethiol/2-mercaptoethanol onto the PM-EDMA film. As shown in Figure 4C, the C 1s peak of the superhydrophobic sample showed two newly formed signals at binding energies of 291.5 eV and 291.9 eV, which belong to the $-CF_2-$ and $-CF_3$ groups of the grafted 1H, 1H, 2H, 2H-perfluorodecanethiol, respectively. Meanwhile, the F 1s high resolution spectrum in Figure 4E also shows the peaks at 688.8 eV and 690.9 eV, well matched with the $-CF_2-$ and $-CF_3$ groups. In Figure 4D, The C 1s high resolution spectrum of superhydrophilic sample displays the peaks on 284.8

eV, 286.3 eV, 287.2 eV and 288.7 eV, which stem from the C-C, C-O, -C-S-C- and C=O bonds. Further, Figure 4F shows S 2p high resolution spectrum of three samples, there was no S peak on PM-EDMA film. In addition, the decline of intensity at ~2120 cm^{-1} (C≡C bond) of superhydrophobic and superhydrophilic samples in the Raman spectroscopy also proves that the reaction occurred between the C≡C bonds and thiols. However, this peak did not totally disappear even after a long time UV irradiation because some of alkyne groups are not accessible on the film surface (**Figure S7**). In summary, all the above analyses confirm that C≡C bond of PM-EDMA film reacts with -SH of thiol solution. As a result, we have successfully prepared superhydrophobic and superhydrophilic samples.

Properties of superwettable micropatterns. As shown in **Figure 5**, PM-EDMA film (A) was selectively reacted with 2-mercaptoethanol by photomask. The reacted regions were transformed into superhydrophilic (B), meanwhile the non-reaction regions reacted with 1H, 1H, 2H, 2H-perfluorodecanethiol and were transformed into superhydrophobic. The superhydrophobic-superhydrophilic micropattern (C) were then created. Several micropattens were prepared to evaluate the mechanical durability and chemical resistance, including water drop test **(Figure 6A)**, sand grain impact test (Figure 6B) and soaking test in acid/alkaline solutions. Figure 6C shows the micropattern photographs of squares and triangles before and after dropping 5000 water droplets from 50 cm height. Figure 6D displays the micropattern photographs of long strips and dots before and dropping 30 g sand grains (average size is 300 μm) from 50 cm height onto the surface. The optical photograph before and after soaking in acid (HCl with pH = 2) and basic (NaOH with pH = 13) solutions for 24 h is shown in Figure 6E and F. After these tests, there was no obvious damage in the patterns, which indicates their good mechanical durability and acid-base resistance.

Acid blue distribution on superwettable sample. **Figure 7** showed the deposition morphology of acid blue droplt after evaporating on superhydrophilic, PM-EDMA film and superhydrophobic samples and there was a comparison with superwettable micropattern sample. In Figure 7A, acid blue droplet is spread over and most of the molecules concentrate on the edge which leaves an irregular ring of solute deposits on the superhydrophilic sample. When WCA is less than 90°, the evaporation of the droplet follows the constant contact radius mode, in which WCA and drop height decrease when the liquid dries. This is driven by by an outward, radial fluid flow during evaporation that occurrs inside a droplet. [48, 49] However, different evaporation rates in the edge and center region driectly resulted in more acid blue molecules transported to the edge region and replenished the liquid that have already been evaporated. Eventually they are deposited in the area of the contact line and form a coffee ring-like stain.[50, 51] The intensity image shows the distance between two edges is around 3.5 mm, and there is a sharp decrease of the intensity from the edge to center, but the intensity at the center is stable.

The stains on the PM-EDMA film (Figure 7B) after the acid blue evaporation is much smaller than on the superhydrophilic interface (Figure 7A), and it shows smallest and round morphology on the superhydrophobic sample (Figure 7C). It was suggested that contact angle hysteresis (CAH) is a major factor to influence droplet evaporation.[52, 53] These two samples have low CAH, and the evaporation process follows the fixed WCA mode, in which the contact line continuously moves inwards. As a result, the acid blue molecules distribute as a circle as the droplet shrinks, forming a ring-like deposit spot on hydrophobic film.[54-56] The result is consistent with the observed deposition intensity: the distance between two edges is 2.2 mm and 1.8 mm on the PM-EDMA film and superhydrophobic sample. This distance gradually decreases from edge to center on PM-EDMA film (Figure 7B). There is a smaller decrease on the superhydrophobic surface, which

means more uniform distribution with increasing WCA (Figure 7C). Besides, the deposit spot have higher intensity than superhyphilic surface, which means a better concentration with increasing WCA.

We prepared superwettable micropatterns with the superhydrophilic dots of the size of 1 mm, as shown in **Figure S8**. Due to the wettability difference, the blue acid droplets only stay on the superhydrophilic dots. As shown in Figure 7D, the acid blue formed a uniform round deposition spot. This can be explained by the coexisitence o recirculating flow induced by Marangoni stress and capillary flows during evaporation. A much smaller contact area, caused higher droplet height, can promote recirculation flow induced by Marangoni. Recirculation flow plays an important role in inhibiting the coffee ring effect and cause the acid blue molecules to be uniformly distributed.[57, 58] Besides, the strenghth of recirculation flow is geater than capillary flows, so it's easy to predict that coffee-ring effect was surpressed and acid blue molecules aggregated together, final forming a uniform deposit spot. This demonstrates that superwettable micropatterns are able to facilitate uniform droplet distribution. In summary, this work finds that the distribution of the acid blue molecules is closely related to the surfaces that the liquids are places. **Figure S9** shows the distribution of acid blue droplet on different wettablity glass samples, the result illustrates the acid blue droplet was pinned in superwettable micropattern and form a regular circle spot, so superwettable dots still have best enrichment effect.

Fluorescence detection of OPA. From the above dissuccsion, due to the enhanced Marangoni effect and high hydrodynamic flow resistance of superhydrophobic region, droplet was evenly distributed in the superhydrophilic microdots and formed a uniform deposition point after evaporation. So the superwettable micropattern provides a convenient and efficient method to enhance spot uniformity, which also become a precondition for reliable OPA-microchip. As an

amine alkaloid reagent, OPA is often used for fluorescence determination of primary amine and peptide bond decomposition. However, when it is distributed in water environment for a long time, it is extremely toxic to human body and aquatic organisms. Therefore, we developed an OPA microchip on Ti substrated based on the superwettable micropattern as described before. As **Figure 8A-C** shows, 2 μL (10^{-2} mol L^{-1}) OPA droplet was added onto superwettable microchips, then OPA molecules were enriched inside superhydrophilic dots after water is evaporated, forming uniform deposit spots. The fluorescent intensity was enhanced as the diameter of the superhydrophilic dots decreased. When the diameter of dots was 400 μm, the microchips showed the highest fluorescence intensity. However, the fluorescence intensity became lower when diameter further decreased because of the aggregation-caused quenching.[59-61]

Therefore, the superhydrophilic dot diameter of 400 μm was applied to investigate the relationship between OPA concentration and fluorescence intensity. As shown in Figure 8D, the fluorescence intensity descends with the decrease of OPA concentration. There is a linear relationship between the fluorescence intensity and OPA concentration from 10^{-7} to 10^{-2} mol L^{-1} with a correlation coefficient of 0.994. In addition, the lowest detection concentration can reach 10^{-7} mol L^{-1}. As shown in **Figure S10**, after the water drop test, this microchip still performed very well without losing its sensitivity. Besides, as **Figure S11** shows, according to the relationship of fluorescence intensity, image color and concentration, we prepared a standard color chart, which can reflect unknown concentrations of OPA. In conclusion, superwettable microchips have better spot uniformity and sensitivity, and possess potential as a sensing microchip using other biomarkers.

Colorimetric detection of glucose. Detection of glucose is significant to the diagnosis and management of diabetes. For human beings, fasting blood glucose values is between 3.8-5.5 mM,

a value between 5.5-7.0 mM may indicate a prediabetes alteration, and it's a symptom of diabetes if fasting value is higher than 11.1 mM. We studied the kinetics of a glucose colorimetric assay on the prepared the superwettable microchips on glass. By taking advantage of the GO_x oxidation of glucose reaction, H_2O_2 is generated, and the glucose content is detected through the H_2O_2 concentration.

The glucose solution ranging from 0 to 50 mM was first prepared. We accomplished the colorimetric detection of glucose through measuring color intensity of the well-controlled micro-droplet. **Figure S12** shows the optical photographs of 0, 2, 4, 8, 10, 25 and 50 mM glucose react with GO_x and KI every 2 min. After measuring by image J, as shown in **Figure 9A**, the intensity curve is a slight sigmoidal, which means the reaction speed is slow for the first 10 min, then rises up, finally reaches a steady state. This is attributed to chromogenic reaction and the intensity values decrease with decrease of glucose concentration. The same experiment was performed on PM-EDMA film and was compared with superwettable microchips. Figure 9B shows an obviously increase intensity and sensitivity when microchips is used. Meanwhile, microchip shows 2 mM detection limit while commercial test paper have a limit of 5 mM.[62] In addition, it only takes 15 min for the color to be totally stable while it requires at least 30 min for a commercial microfluidic-based paper device.[63] Figure 9C shows the final photographs of PM-EDMA film and microchip after adding glucose and GO_x/KI, it's obvious that colour becomes deep with increasing concentration of glucose. In addition, as shown in **Figure S13**, the microchip is reusable for after washing with acetone. As Figure S14 shows, according to the color of each concentration, we also prepared the standard color chart, which can achieve real visual glucose detection.

Conclusion

In conclusion, we have successfully fabricated the well-defined superwettable micropatterns on different substrates via a convenient "click" chemistry. The synthesized microchips exhibit superior mechanical and chemical stability, as well as excellent enrichment effect. Microchip based on titanium shows an excellent sensitivity limit of 10^{-7} mol L^{-1} for OPA detection. Moreover, a rapid, low cost and reusable glass microchip was developed and applied to monitor glucose with a concentration down to 2 mM. The developed method is applicable for a range of other substrates and can be used for the development of advanced micro-sensors.

Acknowledgements

J.Y.H. and H.Y. contributed equally to this work. The authors thank the National Natural Science Foundation of China (21501127 and 51502185) and 111 Project (No. D17005), the Natural Science Foundation of Fujian Province (2019J01256), and the funds from the Priority Academic Program Development of Jiangsu Higher Education Institutions (PAPD).

ASSOCIATED CONTENT

Supporting Information

The Supporting Information is available free of charge on the ACS Publications website at DOI: 10.1021/acsbiomaterials.

The water contact angle of samples; SEM images of different surfaces; Cross-sectional SEM of PM-EDMA film; The WCA of PM-EDMA film modified with 2-mercaptoethanol under the different reaction conditions or functionalized with 2-mercaptoethanol dissolved in different

solvents; The WCA images and the FTIR and Raman spectra of PM-EDMA film with various wettability; The optical image of superwettable micropattern and the acid blue solution before and after evaporation and the intensity analysis; The fluorescence image and intensity of OPA on the microchip after water drop test; The standard color chart of different OPA and glucose concentration; The colorimetric and optical photographs of repeated detection of glucose with different concentration glucose droplet (PDF).

References

(1) Hamilton, W. J.; Seely, M. K., Fog basking by the Namib Desert beetle, Onymacris Unguicularis. *Nature* **1976,** *262*, 284-285. DOI: 10.1038/262284a0.

(2) Malik, F. T.; Clement, R. M.; Gethin, D. T.; Krawszik, W.; Parker, A. R., Nature's moisture harvesters: a comparative review. *Bioinspir. Biomim.* **2014,** *9*, 031002. DOI: 10.1088/1748-3182/9/3/031002.

(3) Ju, J.; Bai, H.; Zheng, Y.; Zhao, T.; Fang, R.; Jiang, L., A multi-structural and multi-functional integrated fog collection system in cactus. *Nat. Commun.* **2012,** *3*, 1247. DOI: 10.1038/ncomms2253.

(4) Chen, H.; Zhang, P.; Zhang, L.; Liu, H.; Jiang, Y.; Zhang, D.; Han, Z.; Jiang, L., Continuous directional water transport on the peristome surface of Nepenthes alata. *Nature* **2016,** *532*, 85-89. DOI: 10.1038/nature17189.

(5) Zheng, Y.; Bai, H.; Huang, Z.; Tian, X.; Nie, F. Q.; Zhao, Y.; Zhai, J.; Jiang, L., Directional water collection on wetted spider silk. *Nature* **2010,** *463*, 640-643. DOI: 10.1038/nature08729.

(6) Wang, S.; Liu, K.; Yao, X.; Jiang, L., Bioinspired Surfaces with Superwettability: New Insight on Theory, Design, and Applications. *Chem. Rev.* **2015,** *115*, 8230-8293. DOI: 10.1021/cr400083y.

(7) Zhang, S. N.; Huang, J. Y.; Chen, Z.; Lai, Y. K., Bioinspired Special Wettability Surfaces: From Fundamental Research to Water Harvesting Applications. *Small* **2017,** *13*, 1602992. DOI: 10.1002/smll.201602992.

(8) Liu, M.; Wang, S.; Jiang, L., Nature-inspired superwettability systems. *Nat. Rev. Mater.* **2017,** *2*, 17036. DOI: 10.1038/natrevmats.2017.36.

(9) Ueda, E.; Levkin, P. A., Emerging applications of superhydrophilic-superhydrophobic micropatterns. *Adv Mater.* **2013,** *25*, 1234-1247. DOI: 10.1002/adma.201204120.

(10) Garrod, R. P.; Harris, L. G.; Schofield, W. C. E.; McGettrick, J.; Ward, L. J.; Teare, D. O. H.; Badyal, J. P. S., Mimicking a Stenocara Beetle's Back for Microcondensation Using Plasmachemical Patterned Superhydrophobic-Superhydrophilic Surfaces. *Langmuir* **2007,** *23*, 689-693. DOI: 10.1021/la0610856.

(11) Hou, Y.; Yu, M.; Chen, X.; Wang, Z.; Yao, S., Recurrent Filmwise and Dropwise Condensation on a Beetle Mimetic Surface. *ACS Nano* **2014,** *9*, 71-81. DOI: 10.1021/nn505716b.

(12) Bai, H.; Wang, L.; Ju, J.; Sun, R.; Zheng, Y.; Jiang, L., Efficient water collection on integrative bioinspired surfaces with star-shaped wettability patterns. *Adv. Mater.* **2014,** *26*, 5025-5030. DOI: 10.1002/adma.201400262.

(13) Ishizaki, T.; Saito, N.; Takai, O., Correlation of cell adhesive behaviors on superhydrophobic, superhydrophilic, and micropatterned

superhydrophobic/superhydrophilic surfaces to their surface chemistry. *Langmuir* **2010,** *26*, 8147-8154. DOI: 10.1021/la904447c.

(14) Oliveira, S. M.; Song, W.; Alves, N. M.; Mano, J. F., Chemical modification of bioinspired superhydrophobic polystyrene surfaces to control cell attachment/proliferation. *Soft Matter*. **2011,** *7*, 8932-8941.DOI: 10.1039/c1sm05943.

(15) Lai, Y.; Huang, J.; Cui, Z.; Ge, M.; Zhang, K.; Chen, Z.; Chi, L., Recent Advances in TiO_2 ‐ Based Nanostructured Surfaces with Controllable Wettability and Adhesion. *Small* **2016**, *12*, 2203-2224. DOI: 10.1002/smll.201501837.

(16) Xing, S.; Harake, R. S.; Pan, T., Droplet-driven transports on superhydrophobic-patterned surface microfluidics. *Lab Chip* **2011,** *11*, 3642-3648. DOI: 10.1039/c1lc20390h.

(17) Manna, U.; Lynn, D. M., Patterning and impregnation of superhydrophobic surfaces using aqueous solutions. *ACS Appl. Mater. Interfacs* **2013,** *5*, 7731-7736. DOI: 10.1021/am4026467.

(18) Geyer, F. L.; Ueda, E.; Liebel, U.; Grau, N.; Levkin, P. A., Superhydrophobic-superhydrophilic micropatterning: towards genome-on-a-chip cell microarrays. *Angew. Chem. Int. Ed.* **2011,** *50*, 8424-8427. DOI: 10.1002/anie.201102545.

(19) Efremov, A. N.; Stanganello, E.; Welle, A.; Scholpp, S.; Levkin, P. A., Micropatterned superhydrophobic structures for the simultaneous culture of multiple cell types and the study of cell-cell communication. *Biomaterials* **2013,** *34*, 1757-1763. DOI: 10.1016/j.biomaterials.2012.11.03.

(20) Lai, Y.; Lin, C.; Wang, H.; Huang, J.; Zhuang, H.; Sun, L., Superhydrophilic–superhydrophobic micropattern on TiO_2 nanotube films by photocatalytic lithography. *Electrochem. Commun.* **2008,** *10*, 387-391. DOI: 10.1016/j.elecom.2007.12.020.

(21) Nishimoto, S.; Sekine, H.; Zhang, X.; Liu, Z.; Nakata, K.; Murakami, T.; Koide, Y.; Fujishima, A., Assembly of self-assembled monolayer-coated Al_2O_3 on TiO_2 thin films for the fabrication of renewable superhydrophobic-superhydrophilic structures. *Langmuir* **2009,** *25*, 7226-7228. DOI: 10.1021/la9011372.

(22) Kostal, E.; Stroj, S.; Kasemann, S.; Matylitsky, V.; Domke, M., Fabrication of Biomimetic Fog-Collecting Superhydrophilic-Superhydrophobic Surface Micropatterns Using Femtosecond Lasers. *Langmuir* **2018,** *34*, 2933-2941. DOI: 10.1021/acs.langmuir.7b03699

(23) Zhang, Y.; Ren, T.; He, J., Inkjet Printing Enabled Controllable Paper Superhydrophobization and Its Applications. *ACS Appl. Mater. Interfaces* **2018,** *10*, 11343-11349. DOI: 10.1021/acsami.8b01133

(24) Lai Y. K.; Pan, F.; Xu, C.; Fuch, H.; Chi, L. F., In Situ Surface‐Modification‐Induced Superhydrophobic Patterns with Reversible Wettability and Adhesion. *Adv. Mater.* **2013**, *25*, 1682-1686. DOI: 10.1002/adma.201203797.

(25) Ito, Y., Surface micropatterning to regulate cell functions. *Biomaterials* **1999,** *20*, 2333-2342. DOI: 10.1016/s0142-9612(99)00162-3.

(26) Feng, W.; Ueda, E.; Levkin, P. A., Droplet Microarrays: From Surface Patterning to High-Throughput Applications. *Adv. Mater.* **2018,** *30*, e1706111. DOI: 10.1002/adma.201706111.

(27) Moon, H. S.; Je, K.; Min, J. W.; Park, D.; Han, K. Y.; Shin, S. H.; Park, W. Y.; Yoo, C. E.; Kim, S. H., Inertial-ordering-assisted droplet microfluidics for high-throughput single-cell RNA-sequencing. *Lab Chip* **2018,** 18, 775-784. DOI: 10.1039/c7lc01284e.

(28) Neto, A. I.; Levkin, P. A.; Mano, J. F., Patterned superhydrophobic surfaces to process and characterize biomaterials and 3D cell culture. *Mater. Horiz.* **2018,** *5*, 379-393. DOI: 10.1039/c7mh00877e.

(29) Leite, Á. J.; Oliveira, M. B.; Caridade, S. G.; Mano, J. F., Screening of Nanocomposite Scaffolds Arrays Using Superhydrophobic-Wettable Micropatterns. *Adv. Funct. Mater.* **2017,** *27*, 1701219. DOI: 10.1002/adfm.201701219.

(30) Oliveira, M. B.; Neto, A. I.; Correia, C. R.; Rial-Hermida, M. I.; Alvarez-Lorenzo, C.; Mano, J. F., Superhydrophobic chips for cell spheroids high-throughput generation and drug screening. *ACS Appl. Mater. Interfaces* **2014,** *6*, 9488-9495. DOI: 10.1021/am5018607.

(31) Xu, T.; Song, Y.; Gao, W.; Wu, T.; Xu, L. P.; Zhang, X.; Wang, S., Superwettable Electrochemical Biosensor toward Detection of Cancer Biomarkers. *ACS Sensors* **2018,** *3*, 72-78. DOI: 10.1021/acssensors.7b00868.

(32) Wu, T.; Xu, T.; Chen, Y.; Yang, Y.; Xu, L.-P.; Zhang, X.; Wang, S., Renewable superwettable biochip for miRNA detection. *Sensor. Actuat. B-Chem.* **2018,** *258*, 715-721. DOI: 10.1016/j.snb.2017.11.109.

(33) Garcia-Cordero, J. L.; Fan, Z. H., Sessile droplets for chemical and biological assays. *Lab Chip* **2017,** *17*, 2150-2166. DOI: 10.1039/c7lc00366h.

(34) Tian, X.; Verho, T.; Ras, R. H. A., Moving superhydrophobic surfaces toward real-world applications. *Science* **2016,** *352*, 142-143. DOI: 10.1126/science.aaf2073.

(35) Si, Y.; Wang, T.; Li, C.; Yu, C.; Li, N.; Gao, C.; Dong, Z.; Jiang, L., Liquids Unidirectional Transport on Dual-Scale Arrays. *ACS Nano* **2018**, 12, 9214-9222. DOI: 10.1021/acsnano.8b03924.

(36) Yang, X.; Song, J.; Zheng, H.; Deng, X.; Liu, X.; Lu, X.; Sun, J.; Zhao, D., Anisotropic sliding on dual-rail hydrophilic tracks. *Lab Chip* **2017,** *17*, 1041-1050. DOI: 10.1039/c7lc00028f.

(37) Shang, L.; Cheng, Y.; Zhao, Y., Emerging Droplet Microfluidics. *Chem. Rev.* **2017,** *117*, 7964-8040. DOI: 10.1021/acs.chemrev.6b00848.

(36) Chen, X., Topology optimization of microfluidics — A review. *Microchem. J.* **2016,** *127*, 52-61. DOI: 10.1016/j.microc.2016.02.005.

(39) Chen, X.; Liu, C.; Xu, Z.; Pan, Y.; Liu, J.; Du, L., An effective PDMS microfluidic chip for chemiluminescence detection of cobalt (II) in water. *Microsyst. Technol.* **2012,** *19*, 99-103. DOI: 10.1007/s00542-012-1551-8.

(40) Chen, X.; Shen, J.; Hu, Z.; Huo, X., Manufacturing methods and applications of membranes in microfluidics. *Biomed. Microdevices.* **2016,** *18*, 104. DOI: 10.1007/s10544-016-0130-7.

(41) Guo, F.; Yang, H.; Mao, J.; Huang, J.; Wang, X.; Lai, Y., Bioinspired fabrication SERS substrate based on superwettable patterned platform for multiphase high-sensitive detecting. *Compos. Commun.* **2018,** *10*, 151-156. DOI: 10.1016/j.coco.2018.09.008.

(42) Song, Y.; Xu, T.; Xu, L. P.; Zhang, X., Superwettable nanodendritic gold substrates for direct miRNA SERS detection. *Nanoscale* **2018,** *10*, 20990-20994. DOI: 10.1039/c8nr07348a.

(43) Yen, T. M.; Zhang, T.; Chen, P.-W.; Ku, T.-H.; Chiu, Y.-J.; Lian, I.; Lo, Y.-H., Self-Assembled Pico-Liter Droplet Microarray for Ultrasensitive Nucleic Acid Quantification. *ACS Nano* **2015,** *9*, 10655-10663. DOI: 10.1021/acsnano.5b03848.

(44) Chen, Y.; Min, X.; Zhang, X.; Zhang, F.; Lu, S.; Xu, L. P.; Lou, X.; Xia, F.; Zhang, X.; Wang, S., AIE-based superwettable microchips for evaporation and aggregation induced fluorescence enhancement biosensing. *Biosens. Bioelectron.* **2018,** *111*, 124-130. DOI: 10.1016/j.bios.2018.04.011.

(45) Chen, Y.; Xu, L. P.; Meng, J.; Deng, S.; Ma, L.; Zhang, S.; Zhang, X.; Wang, S., Superwettable microchips with improved spot homogeneity toward sensitive biosensing. *Biosens. Bioelectron.* **2018,** *102*, 418-424. DOI: 10.1016/j.bios.2017.11.036.

(46) Svec, F.; Fréchet, J. M. J., Kinetic Control of Pore Formation in Macroporou Polymers. Formation of "Molded" Porous Materials with High Flow Characteristics for Separations or Catalysis. *Chem. Mater.* **1995,** *7*, 705-715. DOI: 10.1021/cm00052a016.

(47) Rohr, T.; Hilder, E. F.; Donovan, J. J.; Svec, F.; Fre´chet, J. M. J., Photografting and the Control of Surface Chemistry in Three-Dimensional Porous Polymer Monoliths. *Macromolecules* **2003,** *36*, 1677-1684. DOI: 10.1021/ma021351w.

(48) Hu, H.; Larson, R. G., Analysis of the Microfluid Flow in an Evaporating Sessile Droplet. *Langmuir* **2005,** *21*, 3963-3971. DOI: 10.1021/la047528s.

(49) Girard, F.; Antoni, M. l.; Faure, S.; Steinchen, A. Evaporation and Marangoni Driven Convection in Small Heated Water Droplets. *Langmuir* **2006,** *22*, 11085-11091. DOI: 10.1021/la061572l.

(50) Deegan, R. D.; Bakajin, O.; Dupont, T. F.; Huber, G.; Nagel, S. R.; Witten, T. A., Capillary flow as the cause of ring stains from dried liquid drops. *Nature* **1997,** *389*, 827-829. DOI: 10.1038/39827.

(51) Deegan, R. D.; Bakajin, O.; Dupont, T. F.; Huber, G.; Nagel, S. R.; Witten, T. A., Contact line deposits in an evaporating drop. *Nature* **2000,** *62*, 756-765. DOI: 10.1103/physreve.62.756.

(52) McHale, G.; Shirtcliffe, N. J.; Newton, M. I., Contact-Angle Hysteresis on Super-Hydrophobic Surfaces. *Langmuir* **2004,** *20*, 10146-10149. DOI: 10.1021/la0486584.

(53) Gao, L.; McCarthy, T. J., Contact Angle Hysteresis Explained. *Langmuir* **2006,** *22*, 6234-6237. DOI: 10.1021/la060254j.

(54) Cui, L.; Zhang, J.; Zhang, X.; Li, Y.; Wang, Z.; Gao, H.; Wang, T.; Zhu, S.; Yu, H.; Yang, B., Avoiding coffee ring structure based on hydrophobic silicon pillar arrays during single-drop evaporation. *Soft Matter* **2012,** *8*, 10448-10456. DOI: 10.1039/c2sm26271a.

(55) Yang, Q.; Deng, M.; Li, H.; Li, M.; Zhang, C.; Shen, W.; Li, Y.; Guo, D.; Song, Y., Highly reproducible SERS arrays directly written by inkjet printing. *Nanoscale* **2015,** *7*, 421-425. DOI: 10.1039/c4nr04656k.

(56) Kulinich, S. A.; Farzaneh, M., Effect of contact angle hysteresis on water droplet evaporation from super-hydrophobic surfaces. *Appl. Surf. Sci.* **2009,** *255*, 4056-4060. DOI: 10.1016/j.apsusc.2008.10.109.

(57) Trantum, J. R.; Baglia, M. L.; Eagleton, Z. E.; Mernaugh, R. L.; Haselton, F. R., Biosensor design based on Marangoni flow in an evaporating drop. *Lab Chip* **2014,** *14*, 315-324. DOI: 10.1039/c3lc50991e.

(58) Hu, H.; Larson, R. G., Marangoni Effect Reverses Coffee-Ring Depositions. *J. Phys. Chem. B* **2006,** *110*, 7090-7094.DOI: 10.1021/jp0609232.

(59) Bonn, D.; Eggers, J.; Indekeu, J.; Meunier, J.; Rolley, E., Wetting and spreading. *Rev. Mod. Phys.* **2009,** *81*, 739-805. DOI: 10.1103/RevModPhys.81.739.

(60) Hong Y. N.; Lamab, J. W. Y.; Tang, B. Z., Aggregation-induced emission. *Chem. Soc. Rev.* **2011,** *40*, 5361-5388. DOI: 10.1039/c1cs15113d.

(61) Xu, L. P.; Chen, Y.; Yang, G.; Shi, W.; Dai, B.; Li, G.; Cao, Y.; Wen, Y.; Zhang, X.; Wang, S., Ultratrace DNA Detection Based on the Condensing-Enrichment Effect of Superwettable Microchips. *Adv. Mater.* **2015,** *27*, 6878-6884. DOI: 10.1002/adma.201502982.

(62) Martinez, A. W.; Phillips, S. T.; Butte, M. J.; Whitesides, G. M., Patterned paper as a platform for inexpensive, low-volume, portable bioassays. *Angew. Chem. Int. Ed.* **2007,** *46*, 1318-1320. DOI: 10.1002/anie.200603817.

(63) Martinez, A. W.; Phillips, S. T.; Carrilho, E.; III, S. W. T.; Sindi, H.; Whitesides, G. M., Simple Telemedicine for Developing Regions: Camera Phones and Paper-Based Microfluidic Devices for Real-Time, Off-Site Diagnosis. *Anal. Chem.* **2008,** *80*, 3699-3707. DOI: 10.1021/ac800112r.

Legends

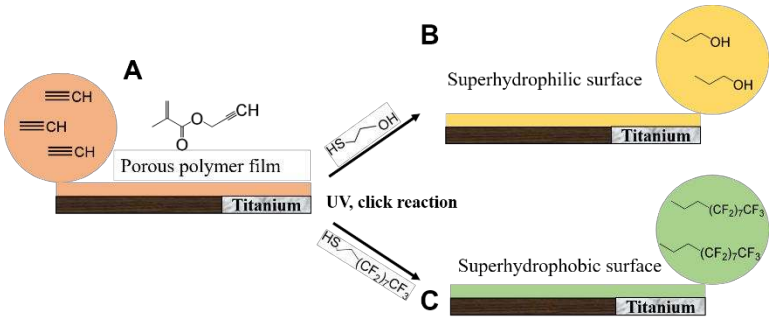

Figure 1. Schematic diagram of reaction process from PM-EDMA film to superhydrophobic sample or superhydrophilic sample.

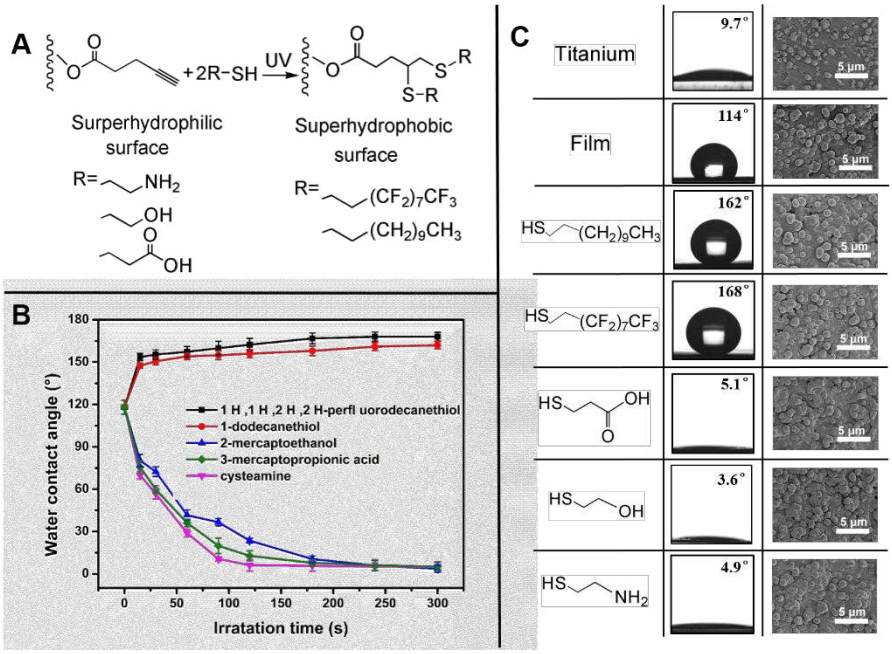

Figure 2. (A) Principle of thiol-yne click chemistry. (B) The WCA of the PM-EDMA film modified with cysteamine (purple), 3-mercaptopropionic acid (blue), 2-mercaptoethanol (green), 1H, 1H, 2H, 2H-perfluorodecanethiol (black), and 1-dodecanethiol (red) via UV irradiation. (C) The WCA and corresponding SEM images: titanium dioxide, PM-EDMA film, as well as PM-EDMA film modified with 1-dodecanethiol, 1H, 1H, 2H, 2H-perfluorodecanethiol, 3-mercaptopropionic acid, 2-mercaptoethanol and cysteamine.

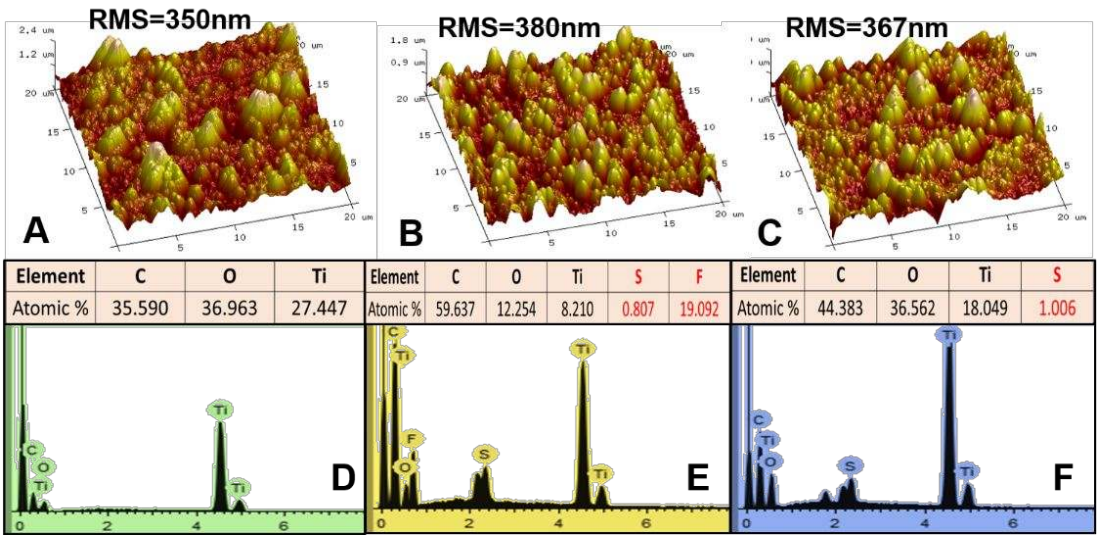

Figure 3. 3D image of AFM of PM-EDMA film (A), superhydrophobic sample (B) and superhydrophilic sample (C). EDS spectrum result shows the element composition of PM-EDMA film (D), superhydrophobic sample (E) and superhydrophilic sample (F).

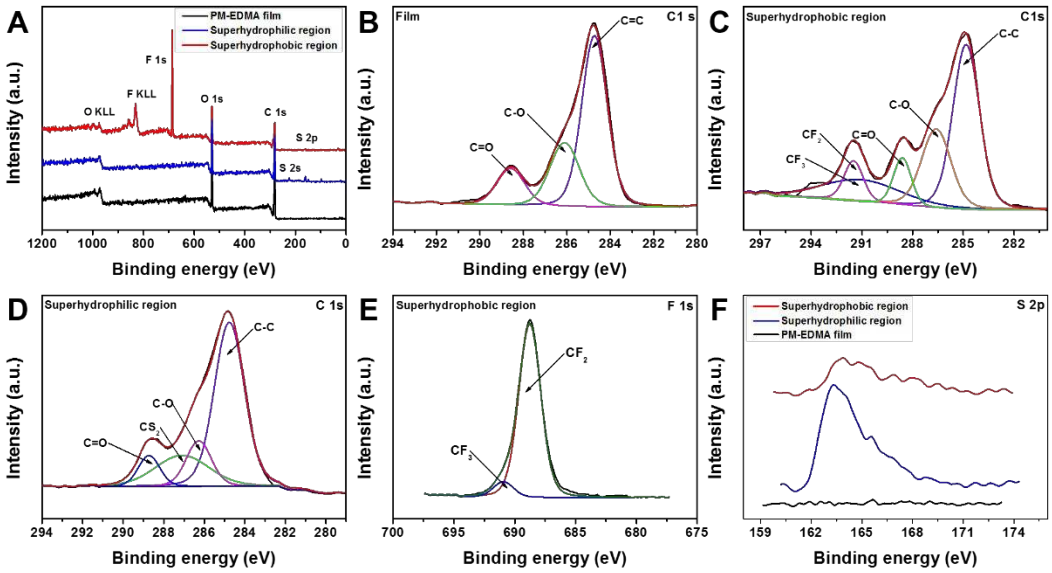

Figure 4. XPS spectra. (A) Wide XPS spectra of PM-EDMA film (black), superhydrophilic surface (blue) and superhydrophobic surface (red). High resolution C 1s spectrum of PM-EDMA film (B), superhydrophobic sample (C) and superhydrophilic sample (D). (E) High resolution F 1s spectrum of superhydrophobic sample. (F) High resolution S 2p spectrum of PM-EDMA film (black), superhydrophilic sample (blue) and superhydrophobic sample (red).

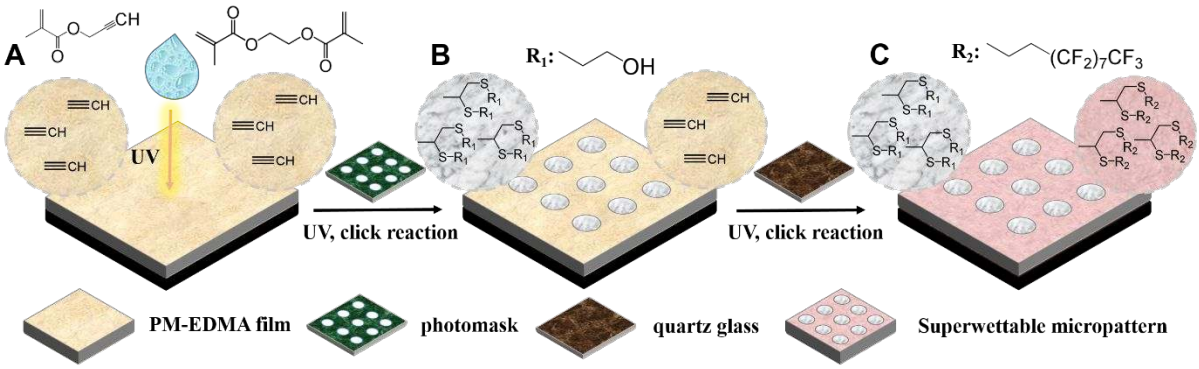

Figure 5. (A) PM-EDMA film. (B) superhydrophilic dot. (C) superhydrophobic-superhydrophilic micropattern.

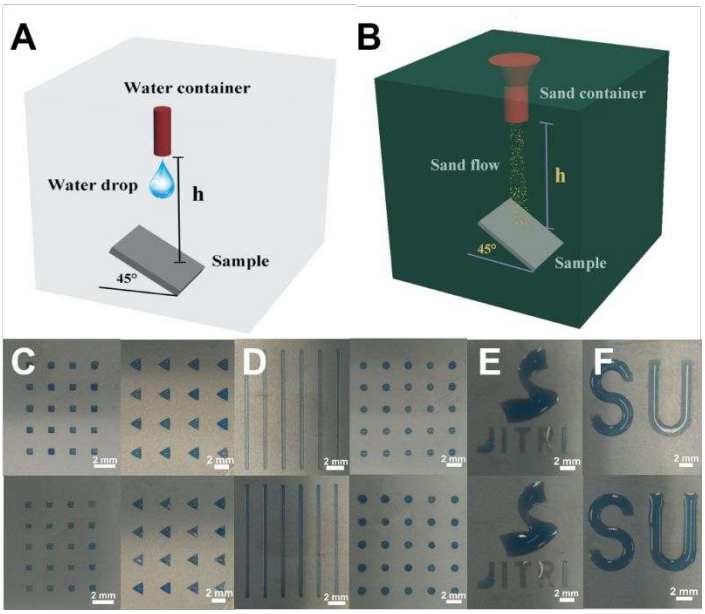

Figure 6. (A) Simple sketch for waterdrop impact test. (B) Simple schematic for sand impact test. (C) Optical photographs of the superwettable micropattern before and after waterdrop impact test. (D) Optical photographs of superwettable micropattern before and after sand impact test. (E) Optical photographs of superwettable micropattern before and after socking in acid solution (pH = 2) for 24 h. (F) Optical photographs of superwettable micropattern before and after dip in basic solution (pH = 13) for 24 h.

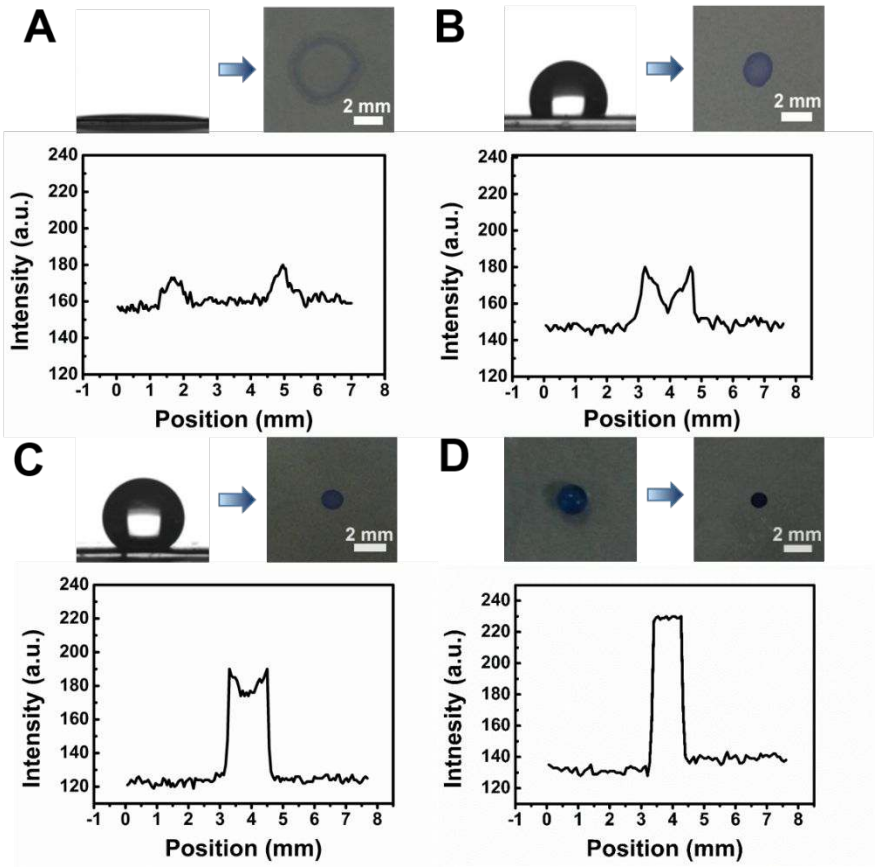

Figure 7. The optical images of acid blue solution (2 μL) after evaporation and the intensity analysis of deposit spots on the superhydrophilic sample (A), PM-EDMA film (B) and superhydrophobic sample (C). (D) The optical images of acid blue solution (2 μL) before and after evaporation and the intensity analysis of deposit spots superwettable micropattern (the diameter is 1 mm).

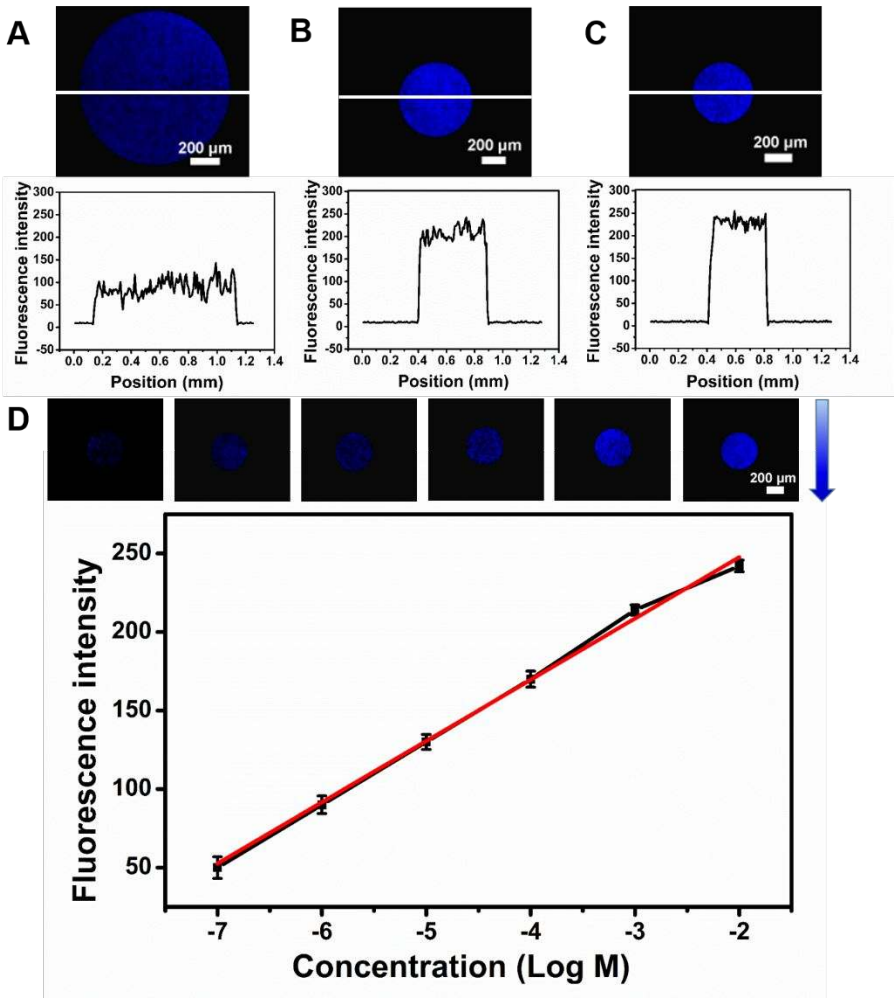

Figure 8. The fluorescence images and fluorescence intensities on the microdots of 1000 μm diameter (A), the microdots of 500 μm diameter (B) and the microdots of 400 μm diameter (C). (D) The fluorescence images and corresponding fluorescence intensity on superwettable microchip with different concentration of OPA.

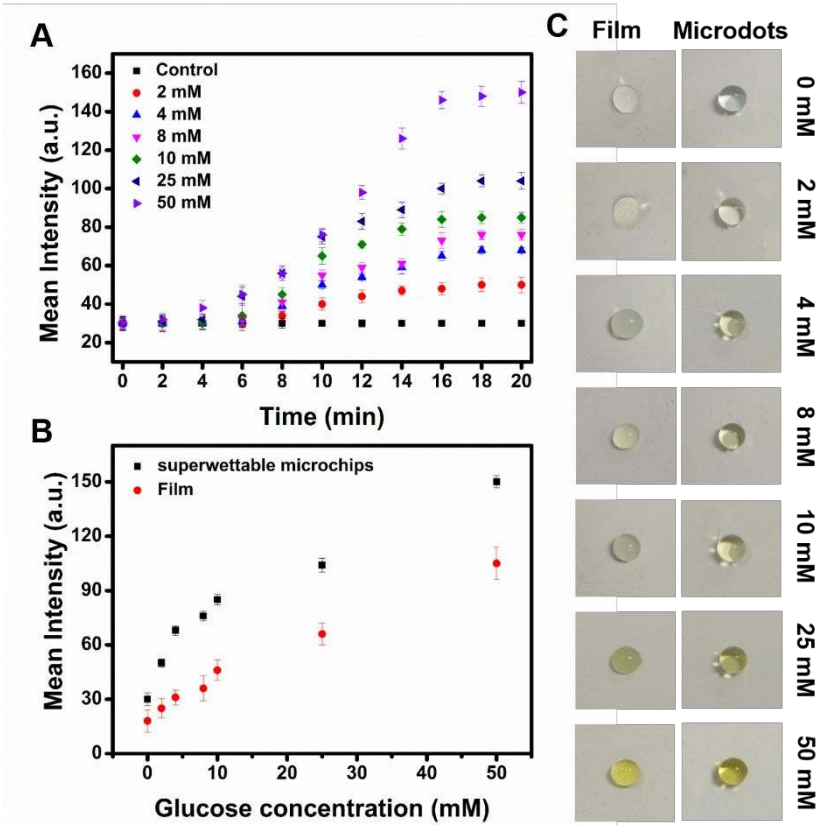

Figure 9. (A) The colorimetric intensity-time image for glucose concentration range of 0-50 mM conducted on microchips. (B) The final intensity comparison between PM-EDMA film and microchip. (C) Top view graphs after 15 min colorimetric reaction on PM-EDMA film and microchip.

For Table of Contents Use Only

Rapid and controllable formation of robust superwettable microchips by click reaction for efficient o-phthalaldehydes and glucose detection

Jianying Huang[a], Hui Yang[a,b], Jiajun Mao[a], Fang Guo[b], Yan Cheng[b], Zhong Chen[c], Xiaoqin Wang[b], Xiao Li[a], Yuekun Lai[a,b*]